Effect of Steel-Fiber Shear Reinforcement on Post-Cracking Shear Fatigue Behavior of Non-stirrup UHPC Beams

Qizhi Xu[1], Yutong Zhu[2], Wendel Sebastian[3], Jingquan Wang[4]

Abstract

Steel fibers in ultra-high performance concrete (UHPC) have been demonstrated to improve resistance to crack growth, decrease deflection, and increase fatigue life under cyclic loads. Using steel fibers as shear reinforcements, this paper investigates its effect on the post-cracking shear fatigue behavior of non-stirrup UHPC beams. The study involved five UHPC beams comprising two static and three fatigue specimens to test the effects of the upper fatigue load, steel-fiber ratio, and stirrup ratio on the shear fatigue response. The test results showed that increasing the initial crack width in the non-stirrup UHPC beam from 0.05 to 0.2 mm (the equivalent of doubling the upper fatigue load) decreased the fatigue life from over two million to 24,875 cycles. The use of steel fibers in place of stirrups increased the residual-to-static strength and residual-to-initial stiffness ratios by 5% and 16%, respectively, after two million cycles. Compared with the specimen with stirrups, the steel-fiber-reinforced specimen had a lower midspan fatigue deflection-to-ultimate static deflection ratio owing to the relieved fatigue strain localization and increased tensile steel reinforcement-UHPC bond fatigue strength. The current codes predict the shear fatigue strength conservatively. A calculation model for accurately predicting fatigue deflection was proposed and compared with the existing test results. A future study on the wider

[1]Lecturer, Civil Engineering Dept, Nanjing Technology University, Nanjing 211816, China. E-mail: qizhixu_seu@163.com.

[2] Master graduate student, Civil Engineering Dept, Southeast University, Nanjing 210096, China. E-mail: 103009228@seu.edu.cn.

[3] Professor, Civil, Environmental and Geomatic Engineering (CEGE). Department, University College London, Chadwick Building, Gower Street, London WC1E 6BT, UK. E-mail: W.Sebastian@ucl.ac.uk.

[4] Professor, Department of Civil Engineering, Southeast University, Nanjing 210096, China. (Corresponding author) E-mail: wangjingquan@seu.edu.cn.

parametric analysis and large-scale beam tests on the fatigue performance of these beams should be conducted.

Keywords Post-cracking shear fatigue; UHPC beam; steel fiber; non-stirrups; damage evolution.

Introduction

For practical engineering applications, some reinforced concrete elements, such as bridge-deck slabs, bridge girders, offshore structures, and wind towers, are commonly subjected to repeated cyclic loading in service. Thus, they are susceptible to fatigue failure by steel reinforcement fracture, concrete crushing with accumulated plastic compressive strain, or excessive crack opening (Gallego et al. 2014; Isojeh et al. 2017a). The shear fatigue failure modes are considered to depend on the shear span-to-depth ratio, shear reinforcement ratio, and fatigue load. However, previous studies primarily focused on the flexural fatigue performance of concrete structures. The shear fatigue response of such beams is yet to be completely understood and hence warrants further study to prevent unexpected brittle failure in practice (Parvez and Foster 2015; Rombach and Kohl 2016).

To improve structural fatigue resistance, the use of high-strength materials has been proposed as a possible solution. Typically, fiber-reinforced polymers (FRP) and ultra-high performance concrete (UHPC) are used to replace steel reinforcements and normal concrete (NC) because of their high strength, superior anti-fatigue, and anti-corrosion performances (El Meski F. and Harajli M. 2015; Li et al. 2015; Peng et al. 2016). In particular, as an advanced material, UHPC has favorable compressive (>150 MPa) and tensile (>7 MPa) strengths, as well as excellent post-cracking behavior (Meng and Khayat 2017; Russell and Graybeal 2013; Shafieifar et al. 2018).

This allows the use of structures with reduced sectional dimensions, lower self-weight, and fewer reinforcements. In this study, a shear-sensitive non-stirrup UHPC thin-web beam was proposed. The live-to-dead load ratio in these beams is significantly increased, thereby resulting in possible shear fatigue failure. Therefore, the study of shear fatigue behavior of non-stirrup UHPC beams is important for advancing material and structural performances, which is beneficial for the cost-effective use of UHPC for long-span lightweight bridges with high durability.

Thus far, very few studies have been conducted on the shear fatigue behavior of NC beams, and even fewer studies have been conducted on UHPC beams. Chang and Kesler (1958a, b) first tested the shear behavior of NC beams without shear reinforcements. Shear compression and diagonal tension failures were observed under repeated cyclic loading. However, these failures do not occur if diagonal shear cracks are not formed. Similar results were observed and demonstrated by Stelson and Cernica (1958) and Frey and Thürlimann (1983). In addition, the shear span-to-depth ratios ranging from 2.0 to 6.36 were further investigated by Higai (1978). The test results indicated that the beam with a ratio of 6.36 failed significantly after the first diagonal crack occurred; however, the fatigue loads could still be borne as the shear span-to-depth ratio decreased to 2.0. Okamura et al. (1981) tested NC beams reinforced with and without stirrups and observed stirrup fractures. The fatigue life increased with an increasing stress ratio and decreasing stress amplitude. Gallego et al. (2014) theoretically found that the concrete in the shear-compression zone was eventually crushed owing to its inability to resist the fatigue load, which could carry approximately 76-88% of the fatigue load, as estimated by Rombach and Kohl (2016).

Compared with NC at the material scale, steel fibers in UHPC could delay crack propagation and increase the fatigue strength by bridging crack surfaces (Carlesso et

al. 2019; Huang and Zhao 1995; Lee and Barr 2004). Therefore, UHPC has the potential to improve structural fatigue performances. Previous studies (Cavagnis et al. 2018; Lee and Barr 2004; Rombach and Kohl 2016) have reported that the presence of steel fibers in steel-fiber-reinforced concrete (SFRC) enhances the fatigue life and reduces the progressive crack growth under fatigue loading. Isojeh et al. (2017a, 2017b) experimentally compared the fatigue performance of NC and SFRC deep beams influenced by the steel fiber contents, stirrup ratio, and longitudinal tensile reinforcement ratio. The specimens failed because of the fracture of the longitudinal steel reinforcements rather than the stirrups, and failure occurred at a shear span-to-depth ratio of 1.25 and a steel fiber ratio of 1.5%. The strut and tie models were modified to predict the fatigue life of the deep beams. Tran (2021) proposed a new approach to further investigate the fatigue degradation of the shear capacity affected by concrete. The experimental-to-calculated ratio of the fatigue shear strength yielded a mean value of 1.02 and a coefficient of variation of 11%. Furthermore, the fatigue behavior of non-stirrup UHPC beams prestressed with FRP tendons was experimentally studied by Fang et al. (2020), in which the shear reinforcements were suggested to be partially omitted, especially for thin-web beams.

Past studies have focused on the fatigue behavior of deep concrete beams, which is affected by shear span-to-effective depth ratios, flexural reinforcement amounts, concrete strengths, and fatigue load magnitudes. The test results indicate that fatigue failure was governed by the fracture of reinforcements for less reinforced beams, whereas the crushing or diagonal tension of concrete occurred for heavily reinforced concrete members. Existing studies have highlighted the potential of steel fibers to enhance the shear fatigue resistance of beams. However, the response and effectiveness of the post-cracking-strain-hardening behavior of UHPC on shear beams

have not been studied in detail. It is also unclear whether steel fibers can replace stirrups.

To date, few experimental studies have been conducted to illustrate the post-cracking shear fatigue behavior of UHPC beams and to determine the function of steel fibers as shear reinforcements to resist shear fatigue loads. Further in-depth studies are required to clarify this issue.

To enrich the existing bank of results, in the present study, two static and three fatigue specimens were tested to determine the effectiveness of steel fibers as shear reinforcements on the post-cracking shear fatigue behavior of such beams. The effects of the upper fatigue-load limit and steel-fiber-replaced stirrups were comprehensively considered in terms of failure modes, fatigue life, fatigue deflection, and strength capacity. A design code-estimated fatigue strength comparison and calculation model for predicting midspan fatigue deflection were also developed. In conclusion, some key conclusions are drawn, and suggestions are made for further work. These results provide insights into the post-cracking shear fatigue behavior of UHPC beams and could lead to an optimized design with reduced section sizes of structural members. Moreover, using steel-fiber reinforcement and enabling simple construction procedures by omitting stirrups result in beams with superior anti-fatigue performance.

Experimental Program

Test Specimens

Five T-shaped specimens with a dimension of 350 × 250 × 60 × 80 × 2200 mm (height × flange width × flange thickness × web thickness × total

length) were tested under four-point loading, comprising two static and three fatigue specimens. All specimens had a clear span length of 2,100 mm between the two supports. The properties and configurations of the tested beams are given in Table 1 and shown in Fig. 1. The web thickness was determined by accommodating 8-mm-diameter stirrups and two bottom 20-mm-diameter longitudinal tensile steel reinforcements. The rib at the midspan was set to maintain the stability of the specimen when the beam sustained a load from a hydraulic jack.

Thus far, no accurate shear span-to-effective depth ratio has been suggested for different failure modes of UHPC beams. Generally, in normal-strength concrete beams, diagonal tension and diagonal compression failures occurred at shear span-to-effective depths of less than 1.0, and above 3.0, respectively, which were prevented by the construction measures in practical engineering as regulated by the current codes (GB 50010-2010 2010). It was at a shear span-to-effective depth ratio ranging from 1.0 to 3.0 that the specimen failed by shear compression. Isojeh et al. (2017) reported that steel-fiber-reinforced concrete deep beams with shear span-to-effective depth ratio below 1.5 may fail owing to the fracture of longitudinal reinforcements rather than shear reinforcements under fatigue loads, whereas the diagonal tension failure was observed for UHPC beams with a shear span-to-effective depth ratio of 3.5 by Fang et al. (2020). Based on previous findings, the shear span-to-effective depth ratio was set to 2.0, to observe the assumed shear-compression failure behavior in the D -region of the UHPC beams. Additionally, non-anchored reinforcing bars were deliberately set to observe whether the beam failed by bond-slip under fatigue loading. It was considered that bond-slip fatigue did not occur if the evolution of the strain differences between the concrete and tensile reinforcement strains was approximately constant. In this study, the strain gauges were not mounted

on the concrete surface near the support. No tensile reinforcement-slipping-induced fatigue splitting cracks (referred to as delaminated cracks), as shown in the failure modes of the static specimens, were observed. It was inferred that the reasonable integrity of the bond between UHPC and tensile steel reinforcements within the shear span has a minor influence on the shear fatigue performance in this study. The use of high-strength concrete, such as UHPC, has been reported to reduce progressive bond loss and increase the stress redistribution (Parvez and Foster 2015). The test results for well-anchored embedded reinforcements previously published by Isojeh et al. (2017) suggested that adequate anchorage, based on code ACI 318 (American Concrete Institute 2014) for steel reinforcements, could preserve the bond strength under fatigue loading. Further investigation is required to determine the minimum anchorage required to ensure reliable bond-slip–anti-fatigue behavior.

In Table 1, the specimens are labeled by the key investigated parameters, which cover two loading types (static and fatigue loading, represented by ST and FA, respectively), two steel-fiber contents (0% and 2%, represented by F0 and F2, respectively), two stirrup ratios (0% and 0.84%, denoted by S0 and S0.84, respectively) and two upper fatigue-load levels (0.25 P_u , 0.5P_u, respectively, where P_u is the ultimate static strength). For example, FA-F2.0-S0-25 refers to a specimen, with 2% steel-fiber content and no stirrups that endured an upper fatigue load of 25% of the ultimate static strength.

The flexural capacity of the tested UHPC beams was designed to be 2.1 times that of the shear capacity to avoid premature flexural failure according to the Chinese code (GB 50010-2010). High-tensile-deformed HRB600 and HRB 400 (GB 50010-2010) steel rebars with nominal yield strengths of 600 and 400 MPa, respectively, were reinforced as longitudinal tensile rebars and stirrups to prevent

flexural fatigue failure. Two deformed HRB400 (GB 50010-2010) steel rebars were placed on the top (hanger bars). The details of the steel reinforcements are shown in Figs. 1 (a) and (b).

The stirrup amount used in the specimen without steel fibers was determined to achieve the same shear resistance (V_{Rd}) as the steel fibers based on the Chinese code CECS38: 2004(CECS 38 2004) as shown in Eqs (1-3), including the contributions from stirrups ($V_{Rd,s}$) and steel fibers ($V_{Rd,f}$). When the steel-fiber volume fractions in the specimens are given, the contributions of the steel fibers to the shear resistance of the UHPC beams can be calculated using Eqs. (2-3). Thereafter, to obtain equal contributions of the steel fibers to the shear resistance, the spacing of the stirrups was determined, based on Eq. 4.

$$V_{Rd} = V_{Rd,f} + V_{Rd,s} + V_c \quad \text{(Eq. 1)}$$

$$V_{Rd,f} = V_c(1 + \beta_v \lambda_f) \quad \text{(Eq.2)}$$

$$V_c = 0.7 f_t b h_0 \quad \text{(Eq.3)}$$

$$V_{Rd,s} = \frac{f_{ywd} A_{sw} h_0}{s} \quad \text{(Eq.4)}$$

where b is the web thickness; h_0 is the effective height; f_t is the tensile strength of the concrete; β_v is set as 0.7 to consider the influence of fiber shape; $\lambda_f = \rho_f l_f / d_f$ is the characteristic value of the steel fiber; ρ_f, l_f and d_f represent the volume fraction, length and diameter of the steel fibers, respectively; f_{ywd} is the yielding strength of the stirrups; A_{sw} is the area of stirrups; and s is the stirrup spacing.

Material Properties

The composition and mechanical properties of UHPC are listed in Table 2. In

this study, the water-to-binder ratio of UHPC was 0.15. It mainly comprised cement (P II 52.5 cement), silica fume, medium-coarse sand, fly ash microspheres, superfine mineral powder, and straight steel fibers of 0.2-mm-diameter and 13- mm-length. A special active admixture SBT®-PCA (Wang et al. 2018), developed by Subote Materials Co. Ltd, was added to the UHPC. This enhanced the concrete workability by obtaining a slump flow of approximately 280 mm and replacing the silica fume with filler materials, such as quartz sand. Thus, the percentage of cement can be reduced to lower both the cost and carbon footprint. Two types of UHPC (types A and B) with steel-fiber volume fractions of 0% and 2% are presented herein.

The UHPC samples representing different material properties were cured at standard room temperature for 28 days. The compressive strength was obtained from three 100 mm cubes and three 100 × 100 × 300 mm prism blocks, whereas three 12.7 × 30 × 80 mm dog-bone samples were used to measure the direct tensile strength of the UHPC. Table 2 lists the average and standard deviation values for the compressive strength of cubes and prisms as 108 ± 1.1 MPa (cube, 0% fiber), 134 ± 3.6 MPa (cube, 2% fiber), 106 ± 5.4 MPa (prism, 0% fiber), and 129 ± 1.5 MPa (prism, 2% fiber). The tensile strengths of dog-bone specimens are listed as 5.2 ± 0.4 MPa (0% fiber) and 7.1 ± 0.8 MPa (2% fiber). The initial elastic moduli tested were 46.7 ± 0.3 GPa and 44.1 ± 1.2 GPa for Type A and B UHPC, respectively. Although UHPC is defined as having a compressive strength of 150 MPa, the required UHPC value in the relevant standards and design guidelines of various countries is recommended to exceed 120 MPa (Yang et al. 2021). In addition, Voo et al. (2010) studied UHPC beams without stirrups and reported a compressive strength of 122-140 MPa. The fatigue crack propagation of the beams depended more on the tensile behavior of the UHPC. Thus, the compressive strength of UHPC (134 MPa in this study) is still considered applicable.

In addition, the yield and ultimate strengths of the HRB600 steel rebars obtained from the tension tests were 662 and 854 MPa, respectively, while those of the HRB400 rebars were 472 MPa and 603 MPa, respectively.

Test Setup and Measurements

Initially, the two beams, ST-F2.0-S0 and ST-F0.0-S0.84, listed in Table 2 were statically tested under four-point loading to determine the ultimate bearing capacity, as shown in Fig. 2(a). The specimens were loaded by force control, and trial loading-unloading cycles were manually performed at 10 kN increments before the shear test to ensure the functionality of all measurements. Subsequently, all specimens were loaded in increments of 10 kN until failure. New cracks were identified, and the loads, strains, and deflection values were recorded at each loading step.

The remaining three specimens were subjected to fatigue tests using a servohydraulic machine with a loading capacity of 500 kN, as illustrated in Fig. 2(b). To prevent possible separation and residual displacements between the transfer steel and testing UHPC beams under cyclic loads owing to their different stiffnesses, the actuator and transfer steel beam were connected by split bolts through a perforated plate, which was also used to connect the tested beam and supports.

The initial crack width considerably affects the fatigue performance of beams (Parvez and Foster 2015). Therefore, it is important to limit the generation of microcracks and crack propagation (Alliche 2004). As suggested by the French code (AFNOR 2016), the maximum crack width is recommended at 0.05–0.2 mm for UHPC members subjected to cyclic loads and wet-dry exposure. Herein the upper fatigue loads were determined based on the loads obtained in the static tests, at which the maximum diagonal crack widths reached 0.05 mm and 0.2 mm, which were tested to 0.25 and 0.5 times the ultimate static loads by measuring the width of each crack.

To ensure that relative displacement did not occur between the actuator and the distributive girder, the lower fatigue load was set to 40% of the upper fatigue load (Fang et al. 2020). Considering the time consumption and high cost of fatigue tests, other parameters, such as fiber dosage, shear span-to-depth ratios, effective depth, and shear reinforcement ratio, were not studied. Two static and three fatigue specimens were tested to observe the effectiveness of using steel fibers to replace stirrups in the post-cracking shear fatigue behavior of UHPC beams. The test results are expected to provide both reference and inspiration for further investigations of the shear fatigue behavior of such beams influenced by other parameters as stated earlier.

During the fatigue tests, the load was first applied monotonically up to the upper fatigue load, and a cyclic load was applied using a sinusoidal wave under load control at a frequency of 3 Hz to avoid overheating of the reinforcing bar (Parvez and Foster 2015). The actuator was programmed to pause at specific intervals to enable data recording and physical observation. The measurements were made after 0.005, 0.01, 0.02, 0.05, 0.1, 0.2, 0.5, 1.0, 1.5, and 2.0 million cycles. If the specimen did not fail after two million cycles, it was monotonically loaded until failure to obtain the residual strength.

The details of the measurements are shown in Fig. 3. Five linear variable displacement transformer (LVDT) sensors (LVDT-1 to LVDT-5, in Fig. 3) were mounted to measure the deflections at the two supporting ends, two loading points, and the midspan of the beam. Moreover, nine strain gauges were uniformly attached to capture the tensile strains of the longitudinal tensile rebars, whereas within the shear span, the strains of the stirrups were measured using three strain gauges attached to each hoop, which were labeled from top to bottom and from slid to pin-supporting. In addition, three gauges were used to measure the outermost compressive and tensile

strains of UHPC within the constant-moment region. Crack widths were measured using a crack microscope with a precision of 0.01 mm. During a particular load cycle, the detected crack tip was marked with an identification number, such that the same crack could be measured in the next load step to obtain the major shear crack width . When the specimen failed, the load was maintained for a few minutes, and two wooden boards were placed on the lateral side of the test set-up to protect the researchers from injury. These risks include possible UHPC portions being expelled from the beam or the sudden collapse of the beam.

Test Results and Discussion

Failure Modes and Crack Patterns

Static Test

The test results are summarized in Table 3, where $\triangle_u$ and V_u refer to the midspan deflection and failure load under static loading, respectively, while V_{upper} and $V_{lower,}$ are the upper and lower fatigue loads, respectively, and $V_{Residual}$ is the residual shear strength. Two failure modes were observed: shear compression (SC) and diagonal compression (DC) failure.

Figs. 4 and 5 show the failure modes and crack patterns, respectively, where the solid lines denote the crack paths, the dashed lines mark the critical diagonal shear cracks, and the numbers indicate the cracks visually observed in order. For specimen ST-F2.0-S0.0, the concrete near the loading point was crushed with pullout steel fibers, and a diagonal shear crack propagated across the entire flange. If the steel fibers were equivalently replaced by stirrups as stated earlier (specimen ST-F0.0-S0.84), the failure mode changed from shear compression to diagonal

compression failure, which typically featured short columns formed in the concrete within the shear span (Fig. 4(b-2)) and finally crushed at the flange of the end support. Additionally, Fig. 4(b-2) shows that the shear and splitting cracks occurred near the support owing to the non-anchored steel rebars and the high shear force.

Table 3 shows that the shear strength increased by 41% when steel fibers were used to replace the stirrups equivalently, indicating that steel fibers were more effective in inhibiting crack propagation and enhancing shear resistance, despite the assumed code-predicted equal strength. The applied loads at which the major crack width was measured 0.05 and 0.2 mm, were tested at 145 and 290 kN, respectively. In contrast, the load for the specimen using stirrups was 103 kN at a crack width of 0.05 mm. A larger crack opening occurred stably after shear crack localization owing to the presence of the steel fibers. Hence, using the initial crack width to determine the fatigue loads was more practical because the structural fatigue behavior was more sensitive to the crack width than the loads, and the function of steel fibers could be evaluated and validated by Wang et al. (2019).

Fatigue Test

Among the three fatigue specimens, FA-F2.0-S0-50 failed by shear compression whereas the remaining specimens did not fail after two million cycles and were subsequently further monotonically loaded until failure. The residual shear strengths of specimen FA-F2.0-S0-25 and FA-F0.0-S0.84-25 were tested for 0.63 and 0.55 times the ultimate static load, indicating that the specimen using steel fibers could achieve better both static and fatigue strengths.

For specimen FA-F2.0-S0-25, when the specimen was subjected to an upper fatigue load, a web-shear crack of 0.05 mm in the shear span formed. Several tightly spaced multiple-cracking flexural cracks were observed in the constant-moment

region. The continuous sound of the steel-fiber slipping was gradually heard after 0.54 million cycles, and the shear crack propagated approximately parallel to the longitudinal reinforcements (denoted as delaminate cracks) at one million cycles. When the load was further cycled up to two million cycles, the delaminate cracks inclined toward the support, and the existing web-shear cracks propagated across the entire web to the top flange.

For specimen FA-F2.0-S0-50, when the upper fatigue load was applied in the first cycle, some flexural-shear and diagonal web cracks gradually appeared within both shear spans. The maximum crack width was 0.2 mm. Flexural cracks were distributed in the constant-moment region and propagated toward 0.8 times a web height. After 20,000 cycles, some diagonal web-shear cracks crossed and intersected, after which they propagated toward the top flange and support. The width of the critical shear crack increased to 1.6 mm, and a combination of pullout and fracture of the steel fibers was observed. As the fatigue load was further increased to 24,000 cycles, the crack in the top flange propagated toward the support and the crack width increased rapidly. After 24,875 cycles, the width of the major web-shear crack increased to 5 mm. New cracks occurred at the bottom surface of the flange and propagated toward the loading point. A sudden shear fatigue failure occurred at the flange near the two loading points.

For specimen FA-F0.0-S0.84-25, some flexural cracks first appeared, after which flexural-shear cracks formed within the shear span, and web-shear cracks developed near the loading points. At the upper fatigue load, the dominant flexural-shear crack width reached 0.2 mm. When the specimen was loaded for 1.85 million cycles, a delamination crack (as defined earlier) occurred at the hanger bars. After the specimen underwent two million cycles, shear fatigue failure did not occur, and many diagonal

shear cracks were observed.

Residual Shear Strength Test after Fatigue Loading

A residual static test was conducted because specimens FA-F2.0-S0-25 and FA-F0.0-S0.84-25 did not fail, even after two million cycles. During the test, the sound of the continuous steel fibers pulling out was heard, and the cracks propagated extensively. At a load of 270 kN, several short, multiple parallel shear cracks were observed within the shear span. Subsequently, the concrete in the flange was crushed under a load of 370 kN. Relative to specimen FA-F2.0-S0-25, a lower failure load of 240 kN was achieved, featuring numerous diagonal cracks and shear compression failures at the top flange.

Load vs Mid-span Deflection Relationships

Fig. 6 shows the load–midspan deflection curves of all the tested specimens. Fig. 6(a) compares the load–midspan deflection curves of the static test, whereas Figs. 6(b–d) show the measured load–midspan deflection curves of the fatigue test.

Fig. 6(a) shows that the beams reinforced with 2% steel fibers had 41% higher shear strength and 43% higher elastic stiffness than those with a stirrup ratio of 0.84%. Therefore, the distributed steel fibers intersecting with diagonal cracks could more effectively inhibit the local opening of shear cracks and thus have substantial potential to entirely replace the stirrups in UHPC beams.

As shown in Figs. 6(b-c), for specimen FT-F2.0-S0-25, the load-deflection curves exhibited two stages. First, the load increased linearly with increasing midspan deflection until the occurrence of a flexural crack (Stage I), after which the stiffness was substantially reduced. Thus, the deflection increased more rapidly than the load (Stage II). It should be noted that the midspan deflection of specimen FT-F2.0-S0-25

increased rapidly before 5,000 cycles, during which the flexural cracks propagated along the cross-sectional height and the diagonal shear cracks increased, progressively reducing the overall sectional flexural stiffness and decreasing the bond stress between the steel fibers and concrete. With the new web-shear cracks observed at shear spans of up to 100,000 cycles, the midspan deflection increased rapidly. Subsequently, a lower increase in deflection was observed for up to two million cycles.

For specimen FT-F0.0-S0.84-25, the midspan deflection increased uniformly before 10,000 cycles, after which it suddenly increased at 20,000 cycles. Subsequently, the midspan deflection increased more rapidly until two million cycles. This was attributed to 20,000 cycles; the formed diagonal shear cracks intersected with each other and generated a critical diagonal shear crack. Increasing the number of cycles resulted in a larger crack width and more participation from the stirrups in resisting the fatigue loads, such that the slope of the load-deflection curves became stable.

Fig. 6(d) shows that the midspan deflection for specimen FT-F2.0-S0-50 increased rapidly before 5,000 cycles, after which the load-deflection curves exhibited elastoplastic characteristics until failure at 24,875 cycles. Relative to specimen FT-F2.0-S0-25, the fatigue life was significantly reduced, and the midspan deflection increased by approximately two times because of the higher load amplitude and larger initial crack width.

Fatigue Damage Evolutions

Midspan Deflection Response

The mid-span deflection and fatigue deflection-to-ultimate static deflection ratios at a particular cycle (W_f/W_{su}) are plotted against the cycle number ratio N/N_f (quotient

of the loading cycle divided by the total cycle number) in Figs. 7(a-b). The deflection increased continuously with increasing N/N_f. The deflection evolution of the specimens behaved similarly and exhibited three stages: elastic deflection (Stage I), elasto-plastic deflection (Stage II), and plastic deflection (Stage III). Within 0 to 0.02, 0.02 to 0.1, and 0.1 to two million cycles, the deflection for specimen FA-F0.0-S0.84-0.25 increased by 26%, 31%, and 30%, respectively, which were approximate to specimen FA-F2.0-S0.0-25 of 23%, 31%, and 20%, respectively.

Fig. 7 shows that at Stage II, specimen FA-F2.0-S0-50 (bearing a higher upper fatigue load and load amplitude) withstood twice as many cycles as specimen FA-F0.0-S0.84-0.25. This indicates that using crack-bridging steel fibers instead of stirrups was beneficial for activating multiple cracks, thereby enhancing the stiffness in Stage II. Additionally, a larger midspan deflection at a specific N/N_f was observed in the specimen using steel fibers, owing to a higher mean fatigue load.

Compared with specimen FA-F2.0-S0-25, specimen FA-F2.0-S0-50 failed with a more rapid increase in deflection under both a higher upper fatigue load and load amplitude. The deflection increased by 22% in stage II ($N/N_f > 0.2$), where multiple new cracks occurred along the beam length, and was smaller than the 45% increase in Stage I ($N/N_f < 0.2$), where initial cracks occurred along the beam depth.

As the cyclic load increased, numerous cracks propagated to the depth of the cross-section, thereby reducing the stiffness of the cracked section. Compared with specimen FA-F0.0-S0.84-25, specimen FA-F2.0-S0.0-25 exhibited a much closer crack spacing, lower crack depth, and smaller maximum crack width in the constant-moment region (see Fig. 5). Fig. 7(a) shows that specimen FA-F2.0-S0-25 had a larger midspan deflection than specimen FA-F0.0-S0.84-25 in the same cycle owing to the higher mean fatigue stress derived from a higher upper/lower fatigue

load. In addition, under a high fatigue load, the steel fibers tended to be pulled out and fractured early, thereby ineffectively reducing the shear span and midspan deflections, although the fatigue life may have been extended. However, Fig. 7(b) shows that the fatigue deflection-to-ultimate static deflection ratio of the fiber-reinforced specimen was smaller than that of the stirrup-reinforced specimen, owing to the larger ultimate static midspan deflection capacity. This indicates that the steel-fiber-reinforced UHPC beams experienced less fatigue damage and could thus resist more cycles.

Maximum Crack Width

The relationship between the maximum shear crack width and load cycles is presented in Fig. 8, where the evolution of crack width behaved similarly and showed three stages: the microcracks continuously formed (Stage I, N/N_f = 0 – 0.02), the macroscopic dominant diagonal crack developed (Stage II, N/N_f = 0.02 – 0.2), and the cracks propagated stably (Stage III, N/N_f >0.2). The lower fatigue load for all specimens was higher than the shear cracking load, hence, the maximum crack width increased rapidly for N/N_f < 0.2, after which a stable increasing stage was observed. This was because the lower amplitude delayed the crack propagation and the occurrence of major diagonal cracks, thereby increasing the fatigue life. At the same N/N_f, a smaller crack width was observed in specimen FA-F2.0-S0-25, despite the 41% higher upper fatigue load. This indicates that with steel fibers, the matrix was beneficial for carrying a higher load and transferring stress to the adjacent uncracked matrix.

Because a two-fold upper fatigue load was applied to specimen FA-F2.0-S0-50, the maximum crack width increased rapidly relative to that of specimen FA-F2.0-S0-25 for N/N_f > 0.2. This was because a major diagonal crack developed after 10,000 cycles and then propagated and opened rapidly under a higher amplitude,

accompanied by UHPC spalling. Finally, the diagonal shear crack reduced the effective depth of the shear-compression region, resulting in shear fatigue failure.

Fatigue Strain in the Steel Reinforcements

The strain developments in the longitudinal reinforcements against the number of cycles are plotted in Figs. 9(a-c). The strain increased almost linearly with the applied load during the specific cycles. Note that none of the longitudinal steel reinforcements fractured after two million cycles. Relative to the strain in the first cycle, at N/N_f = 0.75, the strain increased by 92.2% and 86% for specimens FA-F0.0-S0.84-25 and FA-F2.0-S0.0-25, respectively, whereas a 32.7% increase occurred in specimen FA-F2.0-S0.0-50 at N/N_f= 0.84 owing to the decreased fatigue life at a higher fatigue amplitude. Additionally, Fig. 9(d) compares the strain evolutions of all specimens. The strain of specimen FA-F2.0-S0.0-50 increased stably and then more rapidly than those of the other two specimens. The specimen with steel fibers exhibited a lower strain during the same loading cycle. Because the assumed uniformly dispersed steel fibers significantly increased the strain redistribution capacity and enhanced the bond between the reinforcements and UHPC (Isojeh et al. 2017b), the tension and strain localization over the entire length of the tensile reinforcements were reduced, which decreased the risk of flexural fatigue failure and increased the dowel action might increase to resist a higher shear force and deformation.

In contrast to the neglected post-cracking strength of NC, UHPC exhibited pronounced post-cracking-strain-hardening behavior, in which multiple narrow cracks potentially enabled the effective function of the strain gauge; thus, the measured strain data could be used to evaluate the structural post-cracking behavior. Fig. 8 shows that the crack width increased rapidly after 5,000 cycles, and the tensile strain of the cracked UHPC beam increased by 1963 $u\varepsilon$ relative to the first cycle. Based on the

configuration of the cross-section and plane section assumptions, the strain in the bottom tensile reinforcements reached 6,180 $\mu\varepsilon$, which passed the yielding strain well. However, high-strength tensile reinforcements with a yielding strain and strength of 3,480 $\mu\varepsilon$ and 662 MPa, respectively, were used, which significantly increased the fatigue strength. Additionally, the steel fibers accommodating the beam potentially reduced the stress in the tensile reinforcements, contributing to a reduction in the stress range, thereby surviving more cycles and extending the flexural fatigue life. Further validation is required in the following test using digital image correlation (DIC) technology to capture the strain in UHPC.

Fig. 10 shows the strain evolution of the stirrups. This indicates that the strain increased rapidly in the initial stage (N/N_f<0.1) owing to shear cracking, after which the strain increased stably with cyclic loading. To improve the reliability of the measurements, two gauges were attached to two hoops at the same height in the stirrup, and the electrical strain gauge data obtained were compared at specific intervals during the cyclic loading pause. Additional compensation strain gauges were used to consider the influence of other unstable factors such as temperature to enable accurate measurements. The test results in Fig, 10 confirm that stirrups SS-6 and SS-4 first yielded after 50,000 and 100,000 cycles, respectively, whereas the other stirrups began to yield after one million cycles because the inclined web-shear cracks first formed at the middle of the cross-section within the shear span and propagated across the stirrup. Along with the strain evolution in the longitudinal reinforcements, a larger local strain and crack width were observed in specimen FA-F0.0-S0.84-25, implying potential fatigue failure of the stirrup fracture.

Fatigue Strain in the UHPC

Fig. 11 presents the load versus maximum compressive and tensile strain

evolutions of the midspan cross-section. Owing to the malfunction of the strain gauges attached to the UHPC surface within the shear span, shear strains were not obtained successfully when intersected by concrete cracks. The strain evolution for specimen FA-F0.0-S0.84-25 was truncated after 200,000 cycles, owing to the malfunction of the strain gauge.

The parallel curves show that the compressive strain is much lower than the peak compressive strain of the UHPC of 4,164 $\mu\varepsilon$, as predicted by $(750 f_c^{'})^{0.35}$ (Singh et al. 2017) where $f_c^{'}$ is the peak compressive strength. This indicates that the good anti-fatigue capacity of UHPC led to marginal plastic deformation (and hence, minor damage); thus, a larger shear-compression area was developed to resist the fatigue load. The curve in Fig. 11(a-2) shows that the nonlinear load increased significantly with the strain after 200,000 cycles, indicating an accumulated plastic strain.

As the upper fatigue load increased to 50% of the ultimate static load (specimen FA-F2.0-S0.0-50), the compressive strain increased significantly relative to specimen FA-F2.0-S0.0-25. The load-maximum tensile strain in Fig. 11(b-2) shows the evolution of tensile strain at the bottom surface of the tested beams, which reached 6,825 $\mu\varepsilon$ after 5,000 cycles, approximately equaling the ultimate tensile strain of 7,000 $\mu\varepsilon$ of the UHPC (FHWA 2013; Jia et al. 2022), and thus exhibited a highly nonlinear increase in plastic strain.

Fig. 11(c) shows the compressive and tensile-strain evolutions. In the same cycle, approximate strains were observed for specimens FA-F2.0-S0.0-25 and FA-F0.0-S0.84-25, although the higher upper fatigue load for specimen FA-F2.0-S0-25 might have resulted in a larger accumulated plastic strain. This indicates that the use of steel fibers was more effective in inhibiting local crack propagation and redistributing the stress.

Figs. 11(d-e) show the maximum cross-sectional compressive and tensile strains in UHPC against N/N_f. Three stages were observed as described previously, and specimens FA-F2.0-S0-25 and FA-F0.0-S0.84-25 increased approximately. Despite the higher fatigue load and amplitude of specimen FA-F2.0-S0-50, the compressive strain increased linearly. Fig. 11(e) shows that the maximum tensile strain in the specimens with steel fibers increased linearly, whereas that in the specimen reinforced with stirrups first increased linearly and then suddenly increased steeply. This indicated that the stirrups used to resist the shear force were prone to triggering local strain, hence, the shear fatigue fracture of the stirrups was likely to occur.

Fatigue Deflection Capacity and Stiffness Degradation

Steel fibers were superior in enhancing the fatigue deflection capacity compared to stirrups (see Fig.7 (b)), which can be explained from two aspects. 1) Fatigue failure is generally regarded as a result of microcracks or deficiencies in the microstructure. Over the entire beam length, stirrups were spaced at intervals, and treated as concrete deficiencies, whereby discontinuous distribution and localization of the stress were generated, whereas the steel fibers homogeneously and continuously bridged the crack and relieved the strain localization, leading to a better crack distribution and a higher average effective flexural sectional stiffness. 2) The shear force was predominantly transferred by the compressive strut, leading to the accumulation of plastic compressive strain. The presence of steel fibers intersecting the inclined shear cracks retarded shear strains. Moreover, steel fibers physically increased the fatigue bond strength between the tensile reinforcements and UHPC, whereby their tensile strains were reduced (see Figs. 9(d) and 11(e)), such that the flexural tensile-transverse shear coupling stress in the beam decreased accordingly during the potentially longer fatigue life.

Fig. 12 plots the stiffness reduction (SR) coefficient against the loading cycles, in which SR is defined as the quotient of the stiffness at a specific cycle to that at the first cycle. This shows that about 7% higher stiffness in specimen FA-F2.0-S0-25 occurred than that of specimen FA-F0.0-S0.84-25 after two million loading cycles. In addition, the initial stiffness of specimen FA-F2.0-S0-25 was 8% higher. Therefore, the stiffness of specimen FA-F2.0-S0-25 was approximately 16% higher than that of specimen FA-F0.0-S0.84-25 after two million cycles, implying a greater contribution to the global stiffness from the crack-bridging steel fibers than the stirrups.

Shear-compression fatigue failure occurred in specimen FA-F2.0-S0-50, accompanied by fracture and slipping of the steel fibers as the upper fatigue load and amplitude increased. Note that after 20,000 (N/N_f = 0.8) loading cycles, the global stiffness decreased by 44%, which is less than the two-fold reduction (58%) in specimen FA-F0.0-S0.84-25 with half the upper fatigue load of specimens FA-F2.0-S0-50. This indicates that under a higher fatigue load, the steel fibers were prone to hardening and redistributing the stresses in the matrix.

In this study, only three specimens were used for fatigue tests under different loading regimes. They were all associated with the post-cracking shear fatigue behavior and initial crack evolution. To obtain a reference algebraic equation for predicting post-cracking fatigue stiffness degeneration, only one regression equation was provided to improve reliability. Based on the regression of test results, the SR with loading cycles for the UHPC members was obtained as follows:

$$SR = 0.4272 + \frac{0.53362}{1 + e^{(\lg N - 4.48197)/1.108}} \qquad \text{(Eq. 5)}$$

$$(\rho_f = 2\%;\ L_1/h = 2;\ P_u \leq 0.5\ P_0)$$

where SR is the stiffness reduction coefficient and N is the load cycle, ρ_f is the steel-fiber volume fractions of UHPC, L_1 is shear span length, h is the effective height

of the beams, P_u and P_0 are the upper fatigue and static ultimate loads, respectively.

To date, only a few studies have been conducted on the shear fatigue performance of UHPC beams. In Fig. 12, the test results obtained by Fang et al. (2020) are compared with those obtained using Eq. 5. The average values and standard deviations of the prediction-to-test result ratios are 0.77 and 0.07, respectively. Because both the neglected initial shear cracks and the beneficial inhibition of crack propagation from the prestress force in the study by Fang et al.(2020) relieved the global structural stiffness degeneration, the proposed equation conservatively predicted the stiffness degeneration. With more parametric test data, it is possible to populate these spaces further, and progress to a more reliable function with greater R^2 values.

Stiffness and permanent deformation due to concrete creep have not been studied. As reported by Dong et al. (2021), the creep and crack latent stages account for 20% of fatigue life. With 2% steel fibers by volume, the fatigue damage characterized by stiffness degeneration was 0.48 after two million cycles at a maximum stress level of 0.9. In addition, the fatigue creep of the bond between the concrete and reinforcement was neglected (Tran 2021). Thus, based on the linear fatigue damage law, the fatigue damage was determined to be 9.6%. Given the small number of tests and small specimen size, larger-scale beam tests should be performed.

Residual Static Strength and Deflection Capacity

Specimens FA-F2.0-S0.0-25 and FA-F0.0-S0.84-25 did not fail, even after two million cycles. Subsequently, a static test was conducted to determine the residual strength. Fig. 13 compares the load-midspan deflection curves of the monotonic static and residual strength tests after fatigue loading.

The residual static strength was about 0.63 and 0.58 times the ultimate static

strength of specimens FA-F2.0-S0-25 and FA-F0.0-S0.84-25, respectively. In addition, the maximum crack widths achieved 1.67 and 1.3 times as measured during the static test. The smaller plastic deflection, induced by the relieved fatigue damage in the beams using steel fibers resulted in a higher residual strength.

Fig. 13 also shows that for specimens FA-F2.0-S0-25 and FA-F0.0-S0.84-25, the residual deflection-to-ultimate static deflection ratios were 2.92 and 1.64, respectively. Specimen FA-F2.0-S0-25 began to yield when the midspan deflection exceeded 7.8 mm at a load of 241 kN, which was equal to the failure load and deflection of specimen FA-F0.0-S0.84-25. This further demonstrates that the use of steel fibers enhances fatigue strength and stiffness.

Comparisons of Shear Fatigue Strength Capacity with Design Codes

The fib-Model Code 2010 (fib 2010) presents the following formulation to estimate the relationship between the maximum load cycles N and the maximum load $V_{\max}$ for the reinforced NC members without shear reinforcements:

$$\frac{V_{\max}}{V_{\mathrm{Re}f}} = 1 - \frac{1}{10}\log N \qquad \text{(Eq. 6)}$$

where $V_{\mathrm{Re}f}$ denotes the shear capacity determined without considering the fatigue effect.

The shear strength ($V_{\mathrm{Re}f}$) is expressed as follows:

$$V_{\mathrm{Re}f} = k_v \sqrt{f_c}\, z b_w \qquad \text{(Eq. 7)}$$

$$k_v = \frac{0.4}{1+1500\varepsilon_x}\frac{1300}{1000+k_{dg}z} \qquad \text{(Eq. 8)}$$

$$k_{dg} = \frac{32}{16+d_g} \geq 0.75 \qquad \text{(Eq. 9)}$$

$$\varepsilon_x = \frac{1}{2E_s A_s}\left(\frac{M_E}{z} + V_E\right) \quad \text{(Eq. 10)}$$

where z is the effective shear depth and is determined as $0.9d$ (d is the effective flexural depth); b_w is the member width; f_c is the concrete compressive strength; k_v is the parameter for the Lever II approximation; d_g is the maximum aggregate size and should be taken as zero for f_c larger than 70 MPa; E_s is the reinforcement modulus of elasticity; A_s is the tensile reinforcement area; and M_E and V_E are the applied bending moment and shear force, respectively.

The static shear strength according to Eurocode 2 (Bauwesen 2018) is given by

$$V_{R,e} = 0.18k(100\rho_l f_c)^{1/3} b_w d \geq 0.035k^{3/2} f_c^{1/2} b_w d \quad \text{(Eq. 11)}$$

Parameter k can be determined as：

$$k = 1 + \sqrt{\frac{200}{d}} \leq 2.0 \quad \text{(Eq. 12)}$$

where ρ_l denotes the reinforcement ratio.

Based on (Gallego et al. 2014), the general form of the fatigue shear strength presented in Eurocode 2 (Bauwesen 2018) for N load cycles is as follows:

$$\frac{V_{\max}}{V_{ref}} = C + \frac{\log N}{m}\left(\frac{V_{\min}}{V_{ref}} - C\right) \quad \text{(Eq. 13)}$$

where the values of C and m are 0.9 and 15, respectively. This equation can be rewritten as

$$\frac{V_{\max}}{V_{ref}} = 0.9\left(1 - \frac{1}{15}\log N\right) / \left(1 - \frac{x}{15}\log N\right) \quad \text{(Eq. 14)}$$

where $x = V_{min}/ V_{max}$, and V_{min} and V_{max} are the minimum and maximum shear forces, respectively.

Table 4 shows that the current code-estimated shear strength was much lower

than the maximum fatigue load and residual static load. The MC-2010 expression does not consider the influence of load amplitudes. The differences in the code-estimated shear fatigue strengths of specimens FA-F2.0-S0-25 and FA-F0.0-S0.84-25 were derived from the different compressive strengths of UHPC. Additionally, Eurocode 2 (Bauwesen 2018) does not consider the fatigue of concrete under tension stress, and the fatigue-load ratio has an important influence on shear fatigue strength prediction. The current design codes do not consider the influence of the fatigue-load amplitude or the superior tensile-strain hardening behavior of UHPC, resulting in converse predictive results. An accurate method for predicting the shear fatigue capacity of non-stirrup UHPC beams is required in future studies.

Fatigue Deflection Prediction

The midspan deflections of the beams were calculated as follows (Fang et al. 2020):

$$\mathrm{W}=\sum\int\frac{M\overline{M}}{E_0 I_0}ds+\sum\int\frac{kV\overline{V}}{GA}ds \qquad \text{(Eq. 15)}$$

where E_0 is the elastic modulus of the UHPC, I_0 is the inertial moment of the section, G is the Shear modulus of the UHPC, A is the cross-sectional area of the UHPC beam, and k is the nonuniformity coefficient of the shear stress distribution, which is set to 1.7.

After UHPC cracking, the effective moment of inertia of the cross-section is expressed as follows, based on the American Association of State Highway Officials and Load-and-Resistance Factor Design code (AASHTO 2012):

$$\mathrm{I_e}=(\frac{M_{cr}}{M_a})^3 I_g+[1-(\frac{M_{cr}}{M_a})^3]I_{cr}\le I_g \qquad \text{(Eq. 16)}$$

where I_{cr} denotes the transformed moment of inertia of the cracked UHPC section, I_g

denotes the moment of inertia of the gross concrete section about the centroidal axis, M_a denotes the applied bending moment, and M_{cr} denotes the cracked bending moment of the normal section.

Based on the Chinese code GB/T 31387-2015 (2015) for reactive powder concrete, the influence of steel fibers on the stiffness should be considered as follows:

$$EI_r = EI_e(1+\beta\lambda_f) \quad \text{(Eq.17)}$$

where EI_r is the stiffness of the UHPC beams; β is the influence coefficient of the steel fibers on the stiffness of the beams, set to 0.2 (Fang et al. 2020; Hunan Provincial Housing and Urban-Rural Construction Department 2017); $\lambda_f = \rho_f l_f / d_f$ is the characteristic parameter of the steel-fiber content, and ρ_f, l_f and d_f are the volume fraction, length, and diameter of the steel fibers, respectively.

The midspan deflection of a simply-supported beam under four-point loading can be expressed as follows:

$$W_0 = \frac{(3L^2 - 4a^2)Fa}{48EI_r} + \frac{kFa}{2GA} \quad \text{(Eq.18)}$$

where W_0 is the midspan deflection, F is the external load, L is the beam-span length, and *a is* the shear span length.

Under the constant fatigue-load amplitude, the midspan deflection can be regarded as the sum of the static deflection at the upper fatigue load, calculated using Eq.18, and the additional deflection associated with the accumulated cyclic plastic deflection, which is typically characterized by an S-shaped form based on the test results. This sigmoidal relationship can be expressed as follows:

$$W_{pl,N} = [C_1 - C_2 \ln(\frac{N_f}{N_i} - 1)]W_0 \quad (0 < N_i/N_f < 0.9) \quad \text{(Eq. 19)}$$

$$W_{pl,N} = 0 \quad (N_i/N_f = 0) \quad \text{(Eq. 20)}$$

Fang et al.(2020) tested the shear span/depth ratios, load amplitudes, and steel-fiber content on the mid-span fatigue deflections of non-stirrup UHPC beams. The test results were used to determine the coefficients C_1 and C_2, related to the upper and lower fatigue loads, and the ultimate static load, as follows:

$$C_1 = 0.09e^{3.95\frac{F_{\max}}{F_{u,0}}} \quad \text{(Eq.21)}$$

$$C_2 = 0.664\frac{F_{\min}}{F_{u,0}} + 0.029 \quad \text{(Eq.22)}$$

Therefore, the total midspan deflection (W_{total}) for a specific cycle can be calculated using the following equation for $0 < N/N_f < 0.9$:

$$W_{total} = W_{pl,N} + W_0 \quad \text{(Eq.23)}$$

$$(\rho_f = 1.5\text{-}3\%;\ 2 \leq L_1/h \leq 5.25;\ P_u \leq 0.65\ P_0)$$

where ρ_f is the steel-fiber volume fractions of UHPC, L_1 is the shear span length, h is the effective height of the beams, P_u and P_0 are the upper and static ultimate loads, respectively.

Fig. 14 compares the predicted results from Eq. 23 with the test curves for the four-point bending in this study and the three-point bending tests by Isojeh et al. (2017a). A relatively large deviation was observed for specimen FA-F2.0-S0-50 and the specimens bearing an upper fatigue load exceeding 80% of the static failure load. The influence of steel fibers on the midspan deflection was considered using Eq. 17 but participants did not consider its beneficial function in physically enhancing fatigue behavior. In addition, coefficients C_1 and C_2 in Eq. 19 were also determined regressively, which did not consider the key influences of steel fibers and shear span-to-effective depth ratios. Gallego et al. (2014) reported that the inherent scatter and uncertainties of concrete-related fatigue must be considered. Because a limited

number of test specimens are available for SFRC and UHPC beams in shear, further data on a wider scope of parametric tests should be populated. This will enable a theoretical model to quantify the influence of shear span-to-effective depth ratios, and steel-fiber dosages on the midspan fatigue deflection.

Conclusions

This study focused on the experimentally determined post-cracking shear fatigue behavior of non-stirrup UHPC beams. Five specimens, including two static and three fatigue specimens, were used to study the influence of fatigue-load amplitude, steel-fiber content, and stirrup ratio on the failure modes, fatigue deflection, fatigue strength, and stiffness degeneration. The following conclusions were drawn:

(1) Increasing the initial shear crack width from 0.05 to 0.2 mm decreased the fatigue life from over two million to 24,875 cycles, because the macroscopic dominant diagonal crack formed rapidly at 2% of the exerted loading cycles. The upper fatigue load should not exceed 50% of the ultimate static load to prevent a large decrease in the shear fatigue life of non-stirrup UHPC beams

(2) After two million loading cycles, the residual strength-to-ultimate static strength ratios in the specimens with steel fibers and stirrups were approximately 0.63 and 0.58, respectively, whereas their residual stiffness-to-initial stiffness ratios were 0.52 and 0.47, respectively. This implies that using steel fibers as shear reinforcements could achieve both a higher fatigue strength and stiffness in UHPC beams; however, this should be further confirmed by larger beam tests.

(3) The midspan fatigue deflection and crack width increased in both specimens, whereas an approximately 78% higher ductility was observed for specimens using steel fibers after two million cycles. The use of steel fibers was beneficial for activating multiple cracks, increasing the hardening proportions of the matrix,

and improving the steel reinforcement-UHPC bond capacity.

(4) The current design code-predicted shear fatigue strengths for non-stirrup UHPC beams were too conservative compared with the test results, which demonstrated that the reduced section size enabled the same fatigue strength experienced in conventional larger conventional concrete beams. A calculation model for predicting fatigue deflection was also proposed. This agreed well with the test results; however, it requires further validation using a wider scope of tests, considering the limited data used in this study.

(5) In a future study, key challenges to be addressed to develop non-stirrup UHPC beams with high shear fatigue resistance include exploiting the full potential of steel fibers in resisting shear fatigue loads, performing multiple parametric fatigue tests on steel fiber-matrix interactions, and developing a rational fatigue strength prediction model.

Data Availability Statement

Some or all data, models, or codes that support the findings of this study are available from the corresponding author upon reasonable request.

Acknowledgments

The research was sponsored by the National Natural Science Foundation (52308175, U1943205) and Jiangsu Province Youth Science and Technology Talent Lifting Project (JSTJ-2023-JS002). We would like to extend our thanks for their financial support.

References

AASHTO. 2012. “AASHTO LRFD bridge design specifications.” *Washington, DC*.

AFNOR (Association Française de Normalisation). 2016. “National addition to Eurocode 2—Design of concrete structures: Specific rules for ultra-high performance fibre-reinforced concrete (UHPFRC).” *AFNOR NF P18-710*, Paris: AFNOR.

Alliche, A. 2004. “Damage model for fatigue loading of concrete.” *International Journal of Fatigue*, 26 (9): 915–921. https://doi.org/10.1016/j.ijfatigue.2004.02.006.

American Concrete Institute. 2014. “ACI 318-14: Building Code Requirements for Structural Concrete and. Commentary.” *Farmington Hills*.

Bauwesen, D.-N. 2018. “Final Version of PT1-draft prEN 1992-1-1 2018 D3 (CEN-TC250-SC2 N1358), Eurocode 2: Design of concrete structures - Part 1-1: General rules, rules for buildings.” *bridges and civil engineering structures*.

Carlesso, D. M., A. de la Fuente, and S. H. P. Cavalaro. 2019. “Fatigue of cracked high performance fiber reinforced concrete subjected to bending.” *Construction and Building Materials*, 220: 444–455. https://doi.org/10.1016/j.conbuildmat.2019.06.038.

Cavagnis, F., M. Fernández Ruiz, and A. Muttoni. 2018. “A mechanical model for failures in shear of members without transverse reinforcement based on development of a critical shear crack.” *Engineering Structures*, 157: 300–315. https://doi.org/10.1016/j.engstruct.2017.12.004.

CECS 38. 2004. *Technical Specification for Fiber Reinforced Concrete Structures*.

Chang, T. S., and C. E. Kesler. 1958a. “Fatigue behavior of reinforced concrete beams.” *ACI Structural Journal*, 55 (8). https://doi.org/10.14359/11352.

Chang, T. S., and C. E. Kesler. 1958b. “Static and fatigue strength in shear of beams with tensile reinforcement.” *aci structural journal*, 54 (6).

Dong, S., Y. Wang, A. Ashour, B. Han, and J. Ou. 2021. “Uniaxial compressive

fatigue behavior of ultra-high performance concrete reinforced with super-fine stainless wires." *International Journal of Fatigue*, 142: 105959. https://doi.org/10.1016/j.ijfatigue.2020.105959.

El Meski F. and Harajli M. 2015. "Evaluation of the Flexural Response of CFRP-Strengthened Unbonded Posttensioned Members." *Journal of Composites for Construction*, 19 (3): 04014052. https://doi.org/10.1061/ (ASCE)CC. 1943-5614. 0000516.

Fang, Z., R. Hu, R. Jiang, Y. Xiang, and C. Liu. 2020. "Fatigue Behavior of Stirrup Free Reactive Powder Concrete Beams Prestressed with CFRP Tendons." *Journal of Composites for Construction*, 24 (4): 04020018. American Society of Civil Engineers. https://doi.org/10.1061/(ASCE)CC.1943-5614.0001027.

Fédération internationale du béton (fib). 2010. "Model Code 2010." *Bulletin d'information No. 56 and 57*, (Lausanne, Switzerland,).

FHWA (Federal Highway Administration). 2013. "Design guide for precast UHPC waffle deck panel system, includingconnections." *FHWA-HIF-13-032. Washington, DC: FHWA.*

Frey, R., and B. Thürlimann. 1983. *Ermüdungsversuche an Stahlbetonbalken mit und ohne Schubbewehrung*. Basel: Birkhäuser Basel.

Gallego, J. M., C. Zanuy, and L. Albajar. 2014. "Shear fatigue behaviour of reinforced concrete elements without shear reinforcement." *Engineering Structures*, 79: 45–57. https://doi.org/10.1016/j.engstruct.2014.08.005.

GB 50010-2010. 2010. "Design Code for Concrete Structure."

GB/T 31387-2015. 2015. *Reactive Powder Concrete*. National standards PR China.

Higai, T. 1978. "FUNDAMENTAL STUDY ON SHEAR FAILURE OF REINFORCED CONCRETE BEAMS." *Proceedings of the Japan Society of Civil*

Engineers, 1978 (279): 113–126. Japan Society of Civil Engineers. https://doi.org/10.2208/jscej1969.1978.279_113.

Huang, C., and G. Zhao. 1995. "Properties of steel fibre reinforced concrete containing larger coarse aggregate." *Cement and Concrete Composites*, 17 (3): 199–206. https://doi.org/10.1016/0958-9465(95)00012-2.

Hunan Provincial Housing and Urban-Rural Construction Department. 2017. *Technical specification for reactive powder concrete structures*.

Isojeh, B., M. El-Zeghayar, and F. J. Vecchio. 2017a. "Fatigue Resistance of Steel Fiber-Reinforced Concrete Deep Beams." *ACI Structural Journal*, 114 (5). https://doi.org/10.14359/51700792.

Isojeh, B., M. El-Zeghayar, and F. J. Vecchio. 2017b. "High-cycle fatigue life prediction of reinforced concrete deep beams." *Engineering Structures*, 150: 12–24. https://doi.org/10.1016/j.engstruct.2017.07.031.

Jia, L., Z. Fang, R. Hu, K. Pilakoutas, and Z. Huang. 2022. "Fatigue Behavior of UHPC Beams Prestressed with External CFRP Tendons." *Journal of Composites for Construction*, 26 (5): 04022066. American Society of Civil Engineers. https://doi.org/10.1061/(ASCE)CC.1943-5614.0001261.

Lee, M. K., and B. I. G. Barr. 2004. "An overview of the fatigue behaviour of plain and fibre reinforced concrete." *Cement and Concrete Composites*, 26 (4): 299–305. https://doi.org/10.1016/S0958-9465(02)00139-7.

Li, X., Y.-S. Liang, Z.-H. Zhao, and H.-L. Lv. 2015. "Low-cycle fatigue behavior of corroded and CFRP-wrapped reinforced concrete columns." *Construction and Building Materials*, 101: 902–917. https://doi.org/10.1016/j.conbuildmat.2015.10.063.

Meng, W., and K. Khayat. 2017. "Effects of saturated lightweight sand content on key characteristics of ultra-high-performance concrete." *Cement and Concrete Research*,

101: 46–54. https://doi.org/10.1016/j.cemconres.2017.08.018.

Okamura, H., S. A. Farghaly, and T. Ueda. 1981. “Behaviors of reinforced concrete beams with stirrups failing in shear under fatigue loading” *Proceedings of the Japan Society of Civil Engineers*, 1981 (308): 109–122. Japan Society of Civil Engineers. https://doi.org/10.2208/jscej1969.1981.308_109.

Parvez, A., and S. J. Foster. 2015. “Fatigue Behavior of Steel-Fiber-Reinforced Concrete Beams.” *Journal of Structural Engineering*, 141 (4): 04014117. American Society of Civil Engineers. https://doi.org/10.1061/(ASCE)ST.1943-541X.0001074.

Peng, H., J. Zhang, S. Shang, Y. Liu, and C. S. Cai. 2016. “Experimental study of flexural fatigue performance of reinforced concrete beams strengthened with prestressed CFRP plates.” *Engineering Structures*, 127: 62–72. https://doi.org/ 10. 1016/j.engstruct.2016.08.026.

Rombach, G. A., and M. Kohl. 2016. “Fatigue Strength of Reinforced Concrete Beams without Links under Shear Loads.” *ACI Structural Journal*, 113 (5): 941–950. American Concrete Institute. https://doi.org/10.14359/51688924.

Russell, H. G., and B. A. Graybeal. 2013. “Ultra-High Performance Concrete: A State-of-the-Art Report for the Bridge Community[R].” United States. Federal Highway Administration. Office of Infrastructure Research and Development.

Shafieifar, M., M. Farzad, and A. Azizinamini. 2018. “A comparison of existing analytical methods to predict the flexural capacity of Ultra High Performance Concrete (UHPC) beams.” *Construction and Building Materials*, (172): 10–18.

Singh, M., A. H. Sheikh, M. S. Mohamed Ali, P. Visintin, and M. C. Griffith. 2017. “Experimental and numerical study of the flexural behaviour of ultra-high performance fibre reinforced concrete beams.” *Construction and Building Materials*, 138: 12–25. https://doi.org/10.1016/j.conbuildmat.2017.02.002.

Stelson, T. E., and J. N. Cernica. 1958. “Fatigue properties of concrete beams.” *ACI Structural Journal*, 55(8):255-259.

Tran, N. L. 2021. “Shear model mSM-c for slender reinforced concrete members without shear reinforcement subjected to fatigue loads.” *Engineering Structures*, 233: 111886. https://doi.org/10.1016/j.engstruct.2021.111886.

Voo, Y. L., W. K. Poon, and S. J. Foster. 2010. “Shear Strength of Steel Fiber-Reinforced Ultrahigh- Performance Concrete Beams without Stirrups.” *Journal of Structural Engineering*, 136 (11): 1393–1400. https://doi.org/10.1061/ (ASCE)ST. 1943-541X.0000234.

Wang, J., Q. Xu, Y. Yao, J. Qi, and H. Xiu. 2018. “Static behavior of grouped large headed stud-UHPC shear connectors in composite structures.” *Composite Structures*, 206: 202–214. https://doi.org/10.1016/j.compstruct.2018.08.038.

Wang, Y., X. Shao, and J. Cao. 2019. “Experimental Study on Basic Performances of Reinforced UHPC Bridge Deck with Coarse Aggregates.” *Journal of Bridge Engineering*, 24 (12): 04019119. American Society of Civil Engineers. https://doi. org/10.1061/(ASCE)BE.1943-5592.0001492.

Yang, J., B. Chen, and C. Nuti. 2021. “Influence of steel fiber on compressive properties of ultra-high performance fiber-reinforced concrete.” *Construction and Building Materials*, 302: 124104. https://doi.org/10.1016/j.conbuildmat.2021.124104.

List of Tables

Table 1 Design parameters of tested beams

Specimen ID	UHPC Type	f_{cu} /MPa	ρ_f /%	ρ_s /%	ρ_v /%	s /mm	L_1 /mm	L_1 /h	Load range /kN
ST-F2.0-S0	Type B	134	2.0	2.97	/	/	594	2	Static
ST-F0-S0.84	Type A	108	/	2.97	0.84	150	594	2	Static
FA-F2.0-S0-25	Type B	134	2.0	2.97	/	/	594	2	0.1 – 0.25 P_u
FA- F2.0-S0-50	Type B	134	2.0	2.97	/	/	594	2	0.2 – 0.5 P_u
FA- F0.0-S0.84-25	Type A	108	/	2.97	0.84	150	594	2	0.1 – 0.25 P_u

Note f_{cu} = Compressive strength of standard 100 mm cubes; ρ_f = Steel fibers volume fractions of UHPC; ρ_s=Longitudinal reinforcement ratio; ρ_v= Transverse stirrup ratios; s= Spacing of stirrups; L_1= Distance between the loading points and beam ends; h= Sectional effective height of beams; L_1/h = Shear span ratio; and P_u= shear resistance under static loading.

Table 2 Components and properties of UHPC

Weight mix proportion of UHPC								
UHPC Group	Premix (kg/m^3)		High-active admixture (kg/m^3)		Water-reducing admixture (kg/m^3)	Water （kg/m^3）	Steel fibers （kg/m^3）	V_f
Type-A	2,070		1.855		13	184.5	/	0
Type- B	2,070		1.855		13	184.5	157.66	2%
Mechanical properties								
UHPC	f_{cu} (MPa)		f_{ck} (MPa)		f_t (MPa)		Ec (MPa)	
Group	Mean	SD	Mean	SD	Mean	SD	Mean	SD
Type- A	108	1.1	106	5.4	5.2	0.4	46.7	0.3
Type- B	134	3.6	129	1.5	7.1	0.8	44.1	1.2

Note: V_f = Steel-fiber volume fraction; Mean = Average value; SD = Standard deviation.

Table 3 Summary of test results

Specimen ID	Δ_u (mm)	V_u (kN)	V_{upper} (kN)	V_{lower} (kN)	Fatigue life ($\times 10^4$)	$V_{Residual}$ (kN)	Failure modes
ST-F2.0-S0.0	6.55	580.0	—	—	—	—	SC
ST-F0.0-S0.84	4.74	411.7	—	—	—	—	DC
FA-F2.0-S0-25	—	—	145	58	>200	$0.63V_u$	SC
FA- F2.0-S0-50	—	—	290	116	2.49	—	SC
FA-F0.0-S0.84-25	—	—	103	41.2	>200	$0.58V_u$	SC

Note: SC=Shear compression failure; DC=Diagonal compression failure.

Table 4 Comparison between the tested shear fatigue capacity and code design values

Specimen ID	V_{upper} /$V_{u,\ exp}$	V_{lower} /$V_{u,exp}$	Fatigue life ($\times 10^4$)	$V_{Residual,exp}$/ $V_{u,exp}$	$V_{max,\ fib}$/ $V_{u,exp}$	$V_{max,\ EC\text{-}2}$/ $V_{u,exp}$
FA-F2.0-S0-25	0.25	0.1	>200	0.63	0.17	0.24
FA- F2.0-S0-50	0.5	0.2	2.49	—	0.25	0.24
FA-F0.0-S0.84-25	0.25	0.1	>200	0.58	0.22	0.32

Note: $V_{max,fib}$ and $V_{max,\ EC\text{-}2}$ refer to the shear capacity prediction from the fib-Model Code 2010 and Eurocode 2, respectively, after cyclic loading, whereas $V_{u,exp}$ refers to the tested shear capacity of the beams. V_{upper}, $V_{lower,}$ and $V_{Residual,exp}$ denote the upper fatigue load, lower fatigue load, and tested residual static load, respectively.

List of Figures

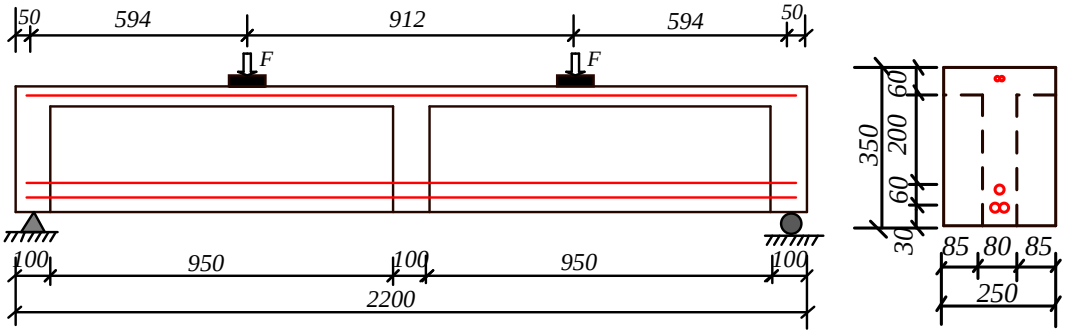

(a) UHPC beams without stirrups

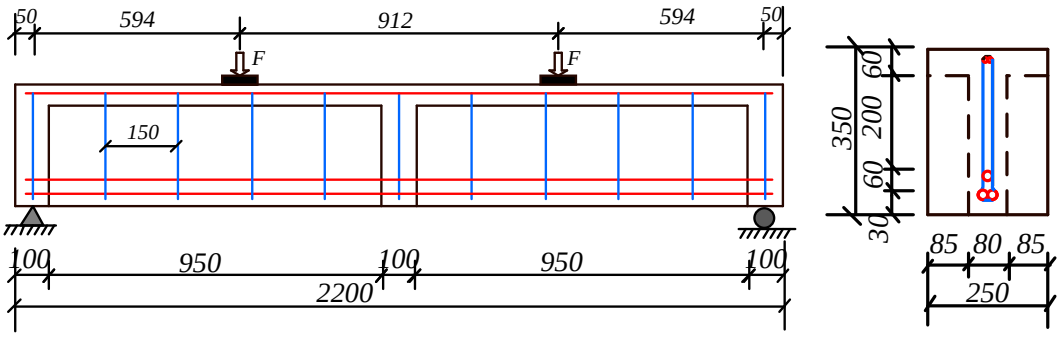

(b) UHPC beams with a 0.84% stirrup ratio

Fig. 1 Dimensions and reinforcements of the tested beams (unit: mm)

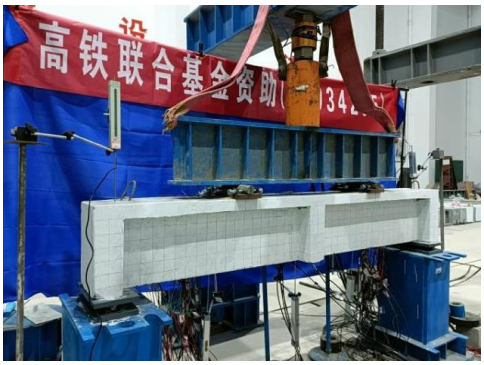

(a) Static test

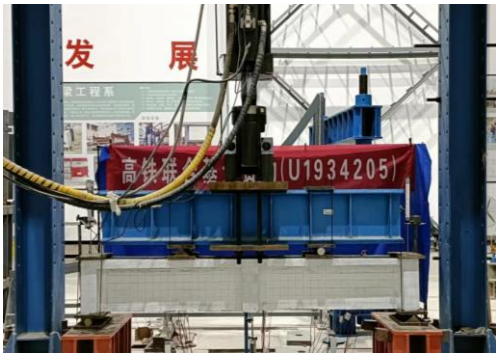

(b) Fatigue test

Fig. 2 Test set-up

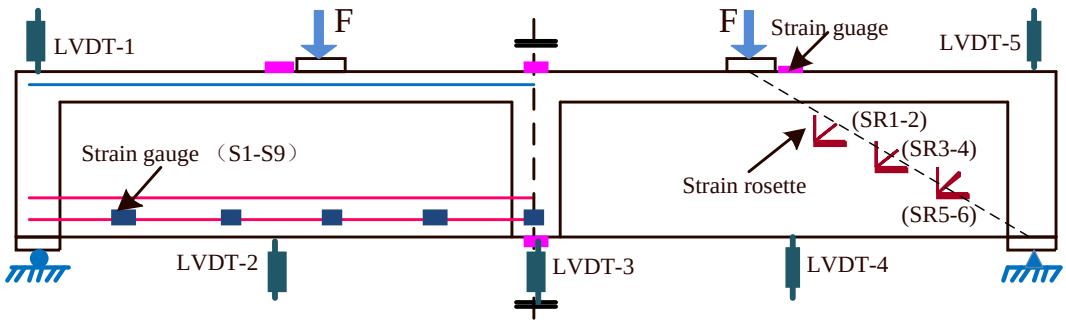

(a) Strain and deflection measurements of non-stirrup beams

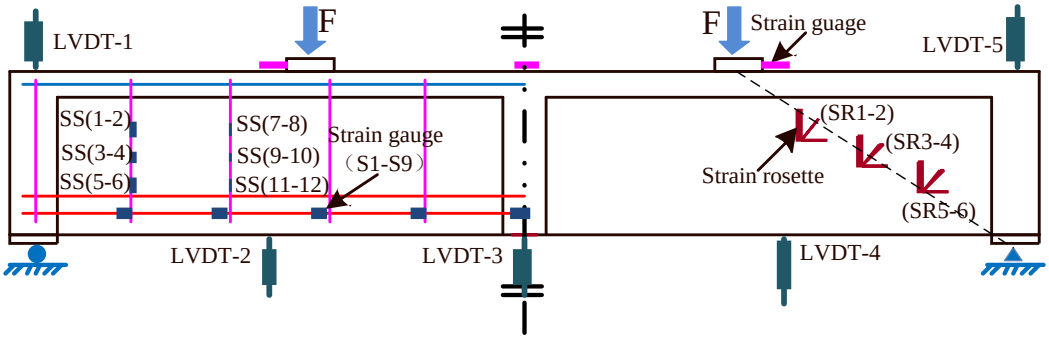

(b) Strain and deflection measurements of beams with stirrups

Fig. 3 Measurement layout of UHPC beams

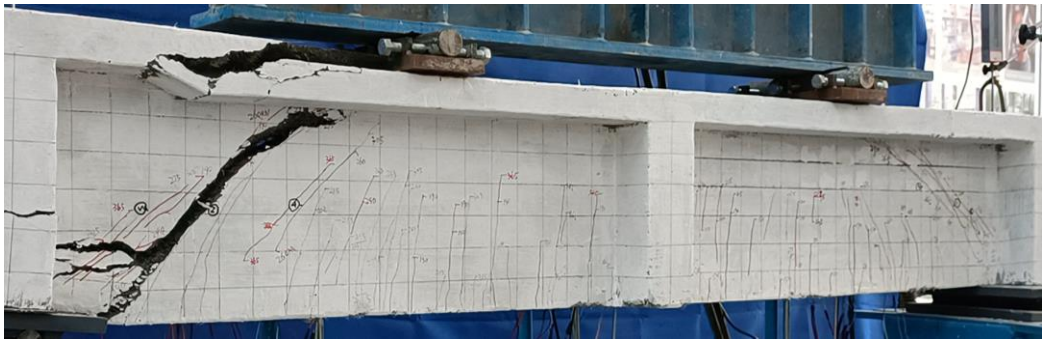

(a) ST-F2.0-S0

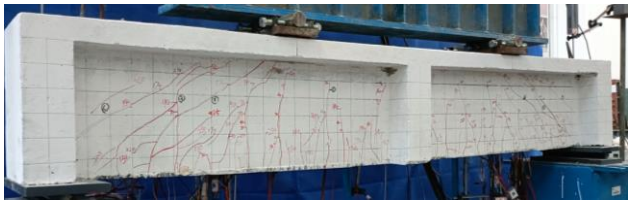

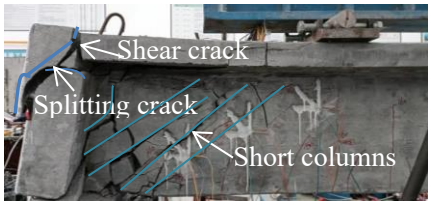

(b-1) Front view of failed beam (b-2) Side view of the failed details

(b) ST-F0.0-S0.84

(c-1) Front view of the failed beam

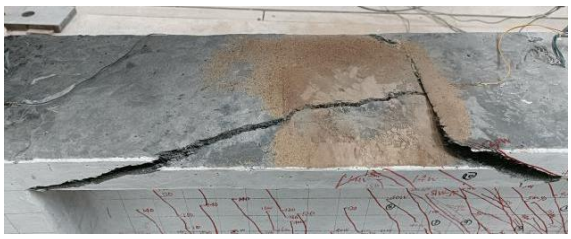

(c-2) Top view of failure detail A (c-3) Top view of failure detail B

(c) FA-F2.0-S0-25

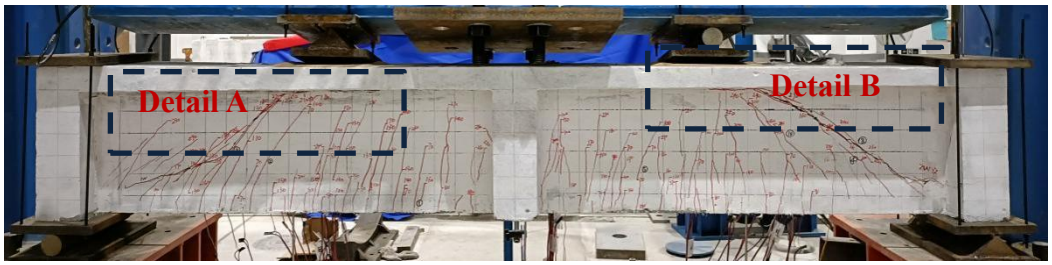

(d-1) Front view of failed beam

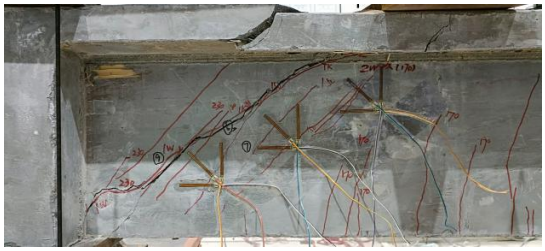

(d-2) Top view of failure detail A (d-3) Top view of failure detail B

(d) FA-F2.0-S0-50

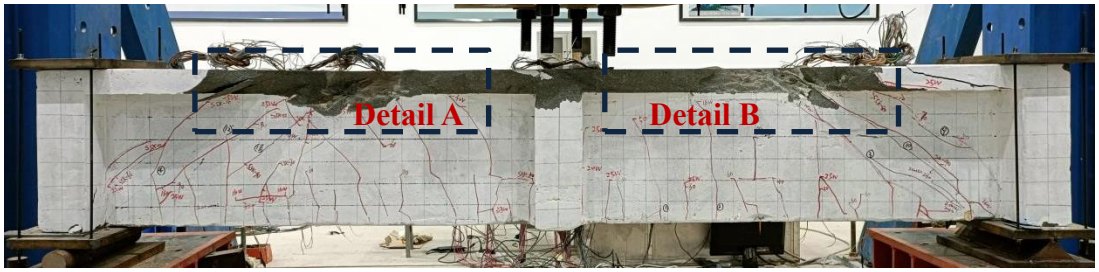

(e-1) Front view of failed beam

(e-2) Back view of failure detail A (e-3) Back view of failure detail B

(e) FA-F0.0-S0.84-25

Fig. 4 Failure modes

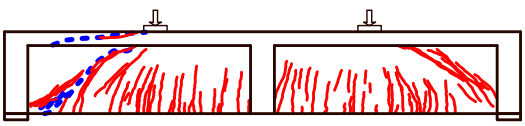

(a) ST-F2.0-S0-R2

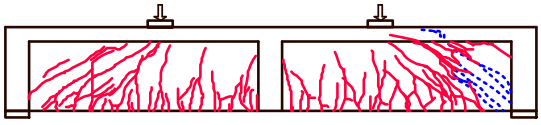

(b) ST-F0.0-S0.8-R

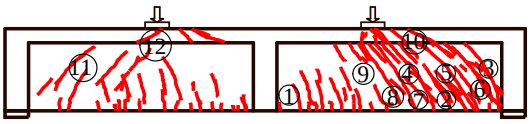

(c-1) FA-F2.0-S0-25 (two million cycles)

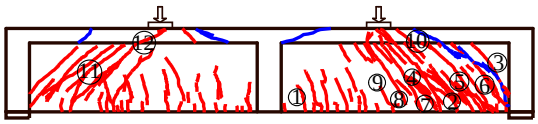

(c-2) FA-F2.0-S0-25 (failure)

(c) FA-F2.0-S0-25

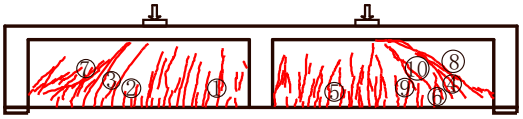

(d-1) FA- F2.0-S0-50 (20,000 cycles)

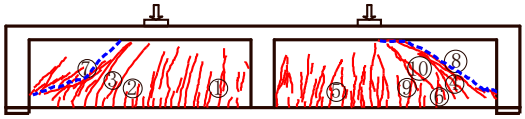

(d-2) FA- F2.0-S0-50 (failure)

(d) FA- F2.0-S0-50

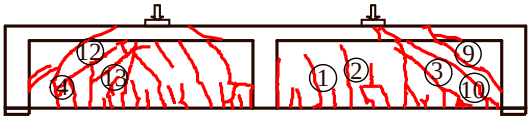

(e-1) FA- F2.0-S0.84-25 (two million cycles)

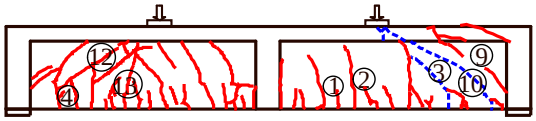

(e-2) FA- F2.0-S0.84-25 (failure)

(e) FA- F2.0-S0.84-25

Fig. 5 Specimen crack patterns

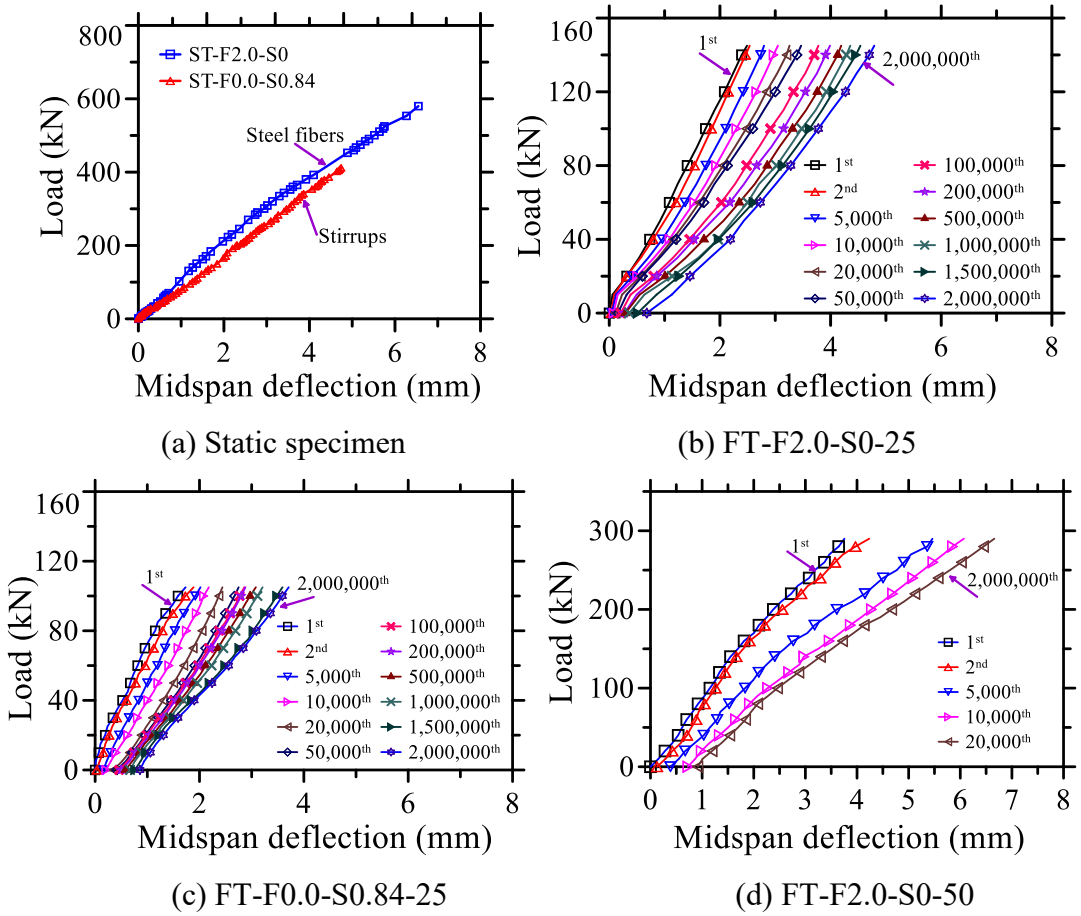

(a) Static specimen

(b) FT-F2.0-S0-25

(c) FT-F0.0-S0.84-25

(d) FT-F2.0-S0-50

Fig. 6 Load-deflection curves of all specimens

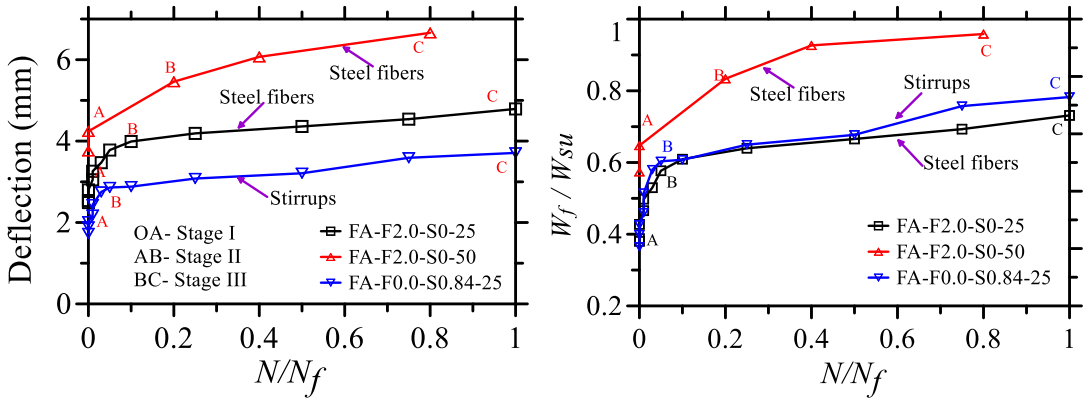

(a) Deflection vs. N/N_f (b) Relative deflection vs. N/N_f

Fig. 7 Midspan deflection vs. N/N_f

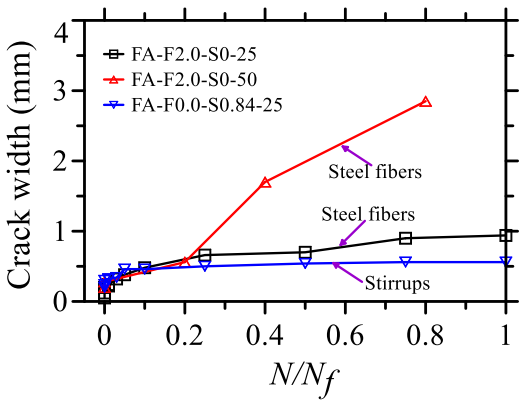

Fig. 8 Maximum crack width vs. N/N_f

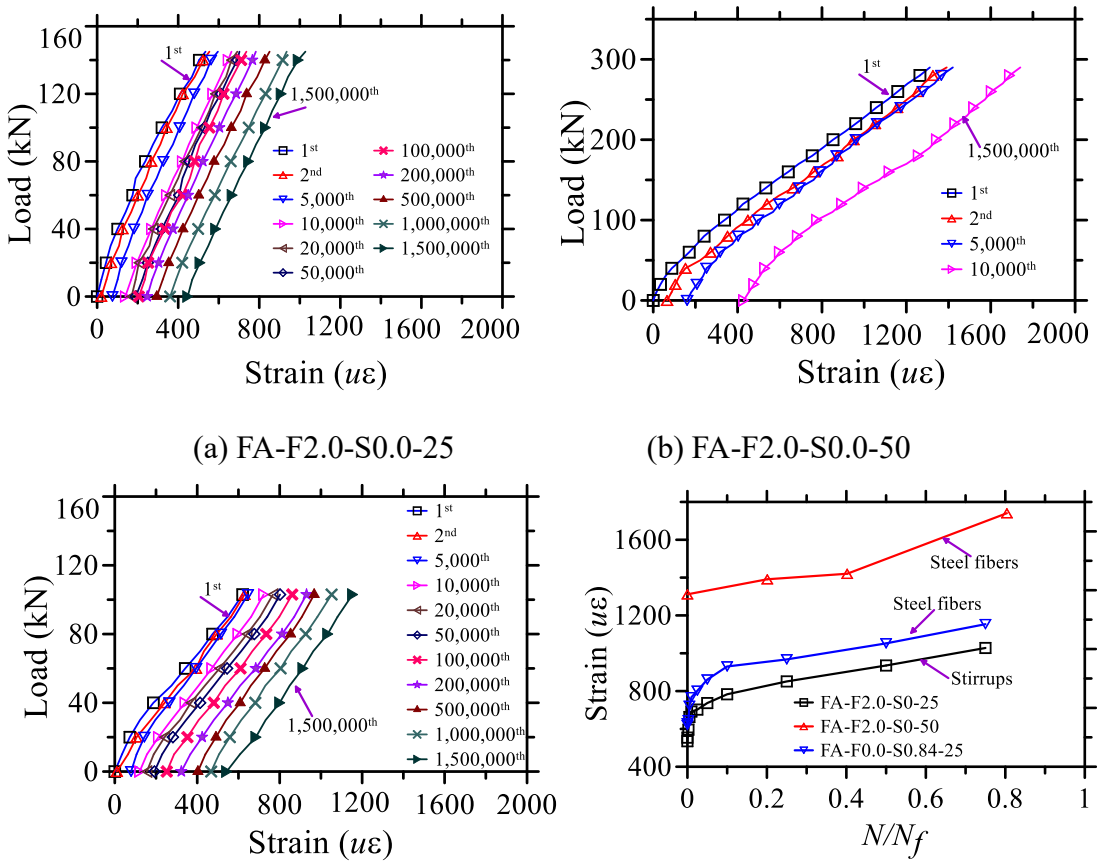

(a) FA-F2.0-S0.0-25 (b) FA-F2.0-S0.0-50

(c) FA-F0.0-S0.84-25 (d) Strain evolution with cycle ratio

Fig. 9 Strain evolution in longitudinal steel reinforcement

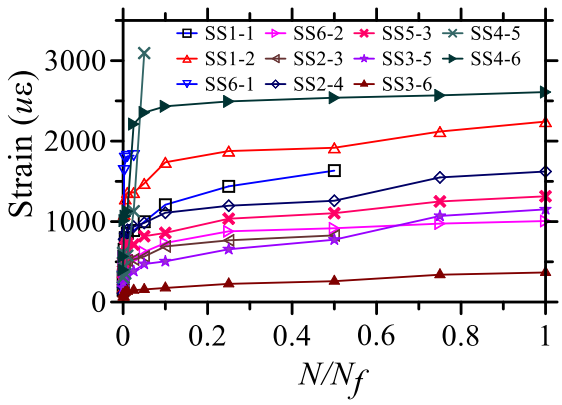

Fig. 10 Strain in stirrups vs. the cycle number ratio N/N_f

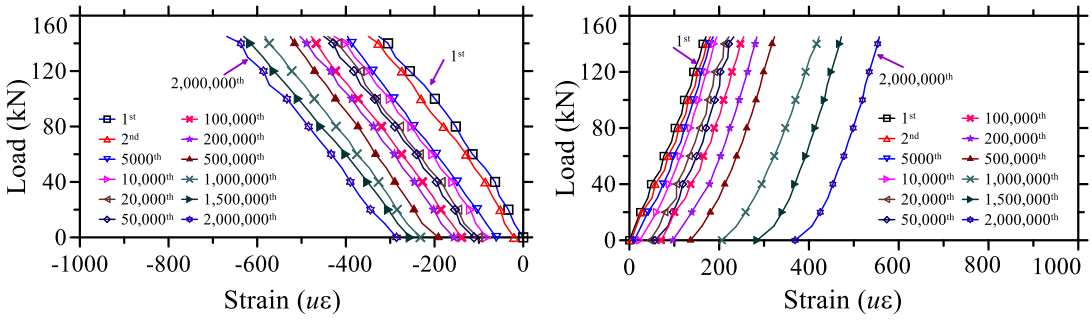

(a-1) Compressive-strain evolution (a-2) Tensile-strain evolution

(a) Specimen FA-F2.0-S0-25

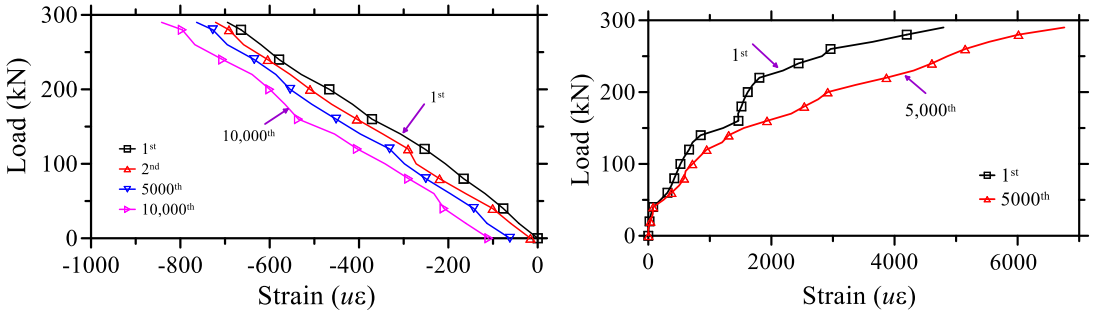

(b-1) Compressive-strain evolution (b-2) Tensile-strain evolution

(b) Specimen FA-F2.0-S0.0-50

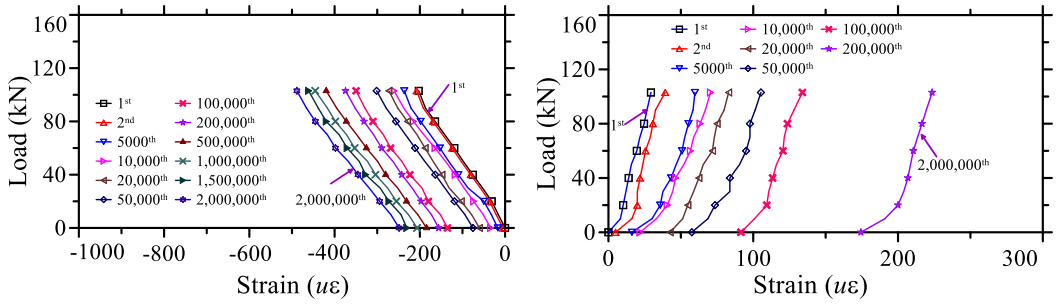

(c-1) Compressive-strain evolution (c-2) Tensile-strain evolution

(c) Specimen FA-F0.0-S0.84-25

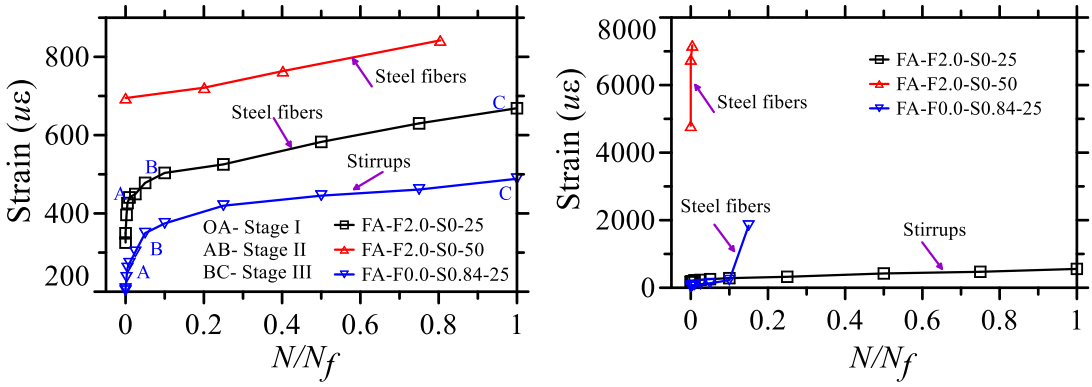

(d) Compressive strain vs. N/N_f (e) Tensile strain vs. N/N_f

Fig. 11 Strain evolutions in UHPC

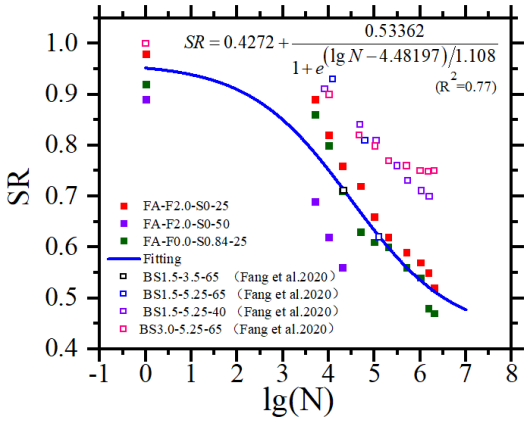

Fig. 12 Stiffness reduction (SR) coefficient vs. loading cycles

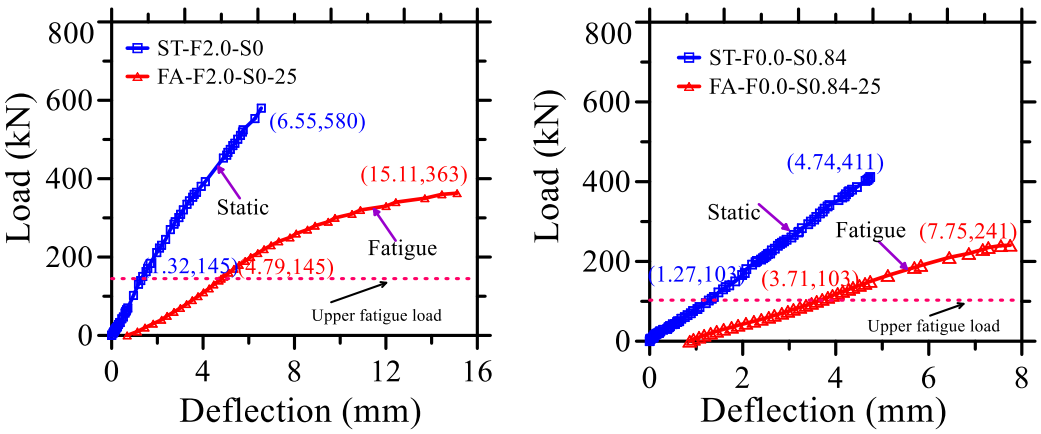

(a) Specimen FA-F2.0-S0-25 (b) Specimen FA-F0.0-S0.84-25

Fig. 13 Load-deflection curves after fatigue loading

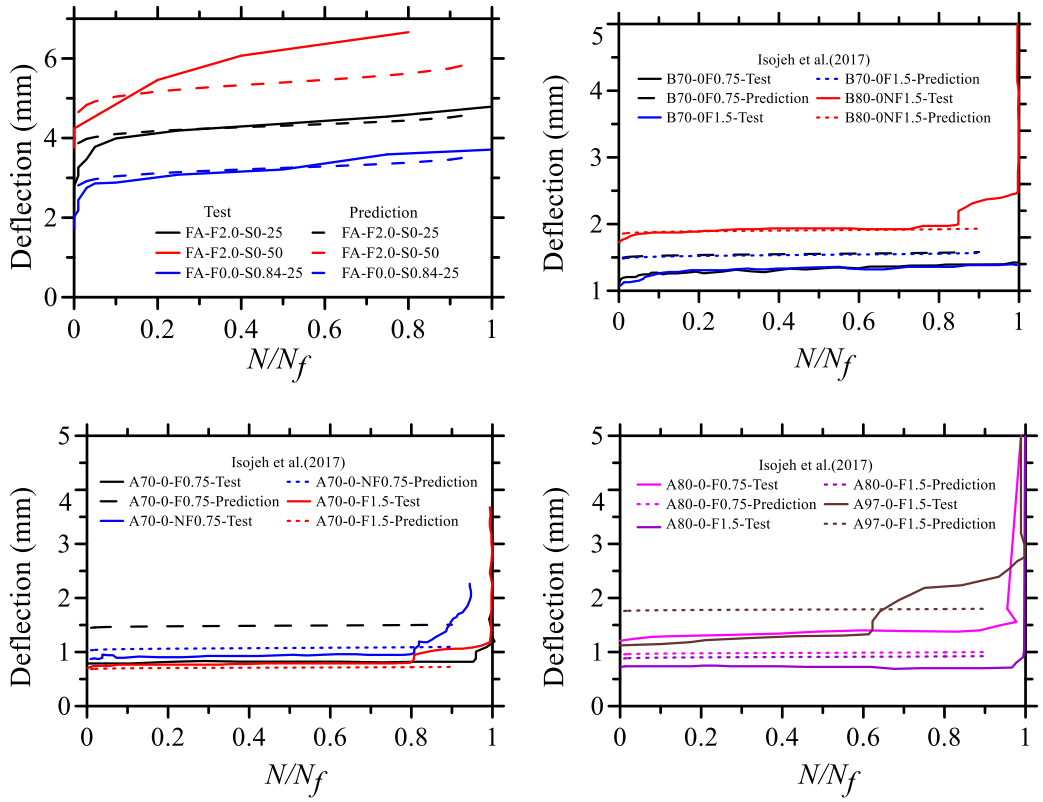

Fig. 14 Comparison between test and calculation results of midspan deflection